Journal of Rock Mechanics and Geotechnical Engineering 5 (2013) 85–96

Journal of Rock Mechanics and GeotechnicalEngineering

Journal of Rock Mechanics and Geotechnical Engineering

journal homepage: www.rockgeotech.org

# Approaches for representing hydro-mechanical coupling between sub-surface excavations and argillaceous porous media at the ventilation experiment, Mont Terri

Alexander Bond [a,*], Alain Millard [b], Shigeo Nakama [c], Chengyuan Zhang [d], Benoit Garritte [e]

[a] Quintessa Ltd., Chadwick House, Birchwood Park, Warrington, Cheshire WA3 6AE, UK
[b] Commissariat à l'Energie Atomique, Yvette, France
[c] Japan Atomic Energy Agency (JAEA), Tokai, Japan
[d] Institute of Rock and Soil Mechanics, Chinese Academy of Sciences, Wuhan, China
[e] Universidad Politécnica de Catalunya, Barcelona, Spain

ARTICLE INFO

*Article history:*
Received 31 March 2012
Received in revised form
19 November 2012
Accepted 10 December 2012

*Keywords:*
Tunnel
Water vapour
Hydro-mechanical (HM) coupling
Numerical modelling
Mont Terri Underground Research Laboratory (URL)
Ventilation experiment (VE)
Argillite

ABSTRACT

At the Mont Terri Underground Research Laboratory (Switzerland), a field-scale investigation has been conducted in order to investigate the hydro-mechanical and chemical perturbations induced in the argillaceous formation by forced ventilation through a tunnel. This experiment has been selected to be used for processing model development and validation in the international project DECOVALEX-2011. The conceptual and mathematical representation of the engineered void, which itself forms a major part of the experiment and is not simply a boundary condition, is the subject of this paper. A variety of approaches have been examined by the contributors to DECOVALEX and a summary of their findings is presented here. Two major aspects are discussed. Firstly, the approaches for the treatment of the surface condition at the porous media/tunnel interface are examined, with two equivalent but differing formulations successfully demonstrated. Secondly, approaches for representing the tunnel with associated air and water vapour movement, when coupled with the hydro-mechanical (HM) representation of the porous medium, are also examined. It is clearly demonstrated that, for the experimental conditions of the ventilation experiment (VE) that abstracted physical and empirical models of the tunnel, can be used successfully to represent the hydraulic behaviour of the tunnel and the hydraulic interaction between the tunnel and the surrounding rock mass.



## 1. Introduction

The capability of a proponent of a radioactive waste disposal facility in a deep geological formation to demonstrate short- and long-term environmental safety is controlled, to a large extent, by the ability to exhibit a good fundamental understanding of the evolution of the system under construction, disposal and closure conditions. Demonstration and development of such an understanding is not a trivial task and by necessity involves experimental investigations which are conducted both in the field as well as in devoted underground research laboratories (URLs). The use of physical models and computer codes that describe and predict the outcomes of such experiments are critical in building confidence that those experimental results can be understood and extrapolated to the spatial and temporal scales required in a full disposal system. Among different possible host rocks, claystone is being investigated by several countries. In Switzerland, the Mont Terri URL was created in 1995 in the Opalinus clay, an argillite formation, in order to characterise and study the geological, hydrogeological, geochemical, and geotechnical properties of this potential host rock. Of the many experiments at the URL, the ventilation experiment (VE) has been carried out in a micro-tunnel to study the processes which may occur due to the controlled ventilation of excavated structures, during the construction and operational phases of the repository. In particular, the water desaturation is expected to change the hydro-mechanical (HM) behaviour of the rock, thus influencing the potential performance and safety of a repository based on similar design concepts.

One task of the international project DECOVALEX-2011 relates to predicting phenomena observed during this experiment. The

* Corresponding author. Tel.: +44 01925 885951.
*E-mail address:* alexbond@quintessa.org (A. Bond).

Peer review under responsibility of Institute of Rock and Soil Mechanics, Chinese Academy of Sciences.

Production and hosting by Elsevier

1674-7755 
http://dx.doi.org/10.1016/j.jrmge.2013.02.002

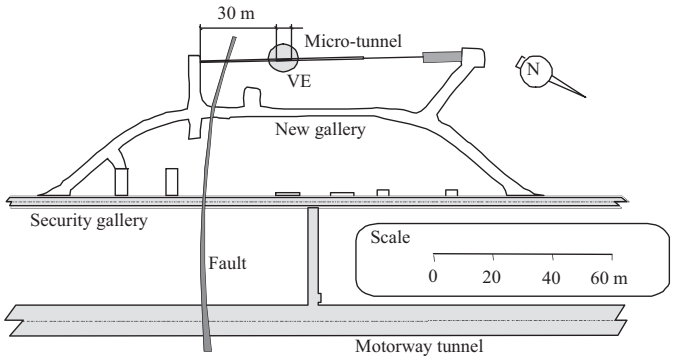


**Fig. 1.** Location of the micro-tunnel in Mont Terri.

task was composed of two broad components. A preliminary task considered modelling a laboratory drying test, in order to evaluate the ability of the computer codes to reproduce the main phenomena involved in the VE, and to identify a first set of hydraulic parameters relevant to the Opalinus clay. Then in the second part of the task, the three different phases of the VE itself have been simulated: a first period (Phase 0) following the excavation of the micro-tunnel in 1999, up to the installation of doors that allow controlled ventilation of a portion of the micro-tunnel, and then a single resaturation–drying cycle (Phase 1) finished in January 2004. This was then followed by further desaturation–resaturation cycles to the end of 2010, although data were only made available for this analysis (both descriptive and predictive) from May 2003 to April 2007. This paper considers the issues surrounding the hydraulic interaction of the rock mass and the tunnel itself.

The basic conceptual model and relevant data are discussed in Sections 2 and 3. Section 4 discusses the techniques used to represent the surface condition for the drying test and VE, while Section 5 examines the different approaches to modelling the tunnel itself, given that for the purposes of this experiment, the tunnel was considered to be part of the experiment and not simply a prescribed boundary condition. Concluding remarks and other observations are given in Section 6.

Contributions to the modelling work presented in this paper were made by individuals from Quintessa Ltd., Commissariat à l'Énergie Atomiqueet aux énergies alternatives (CEA), Japanese Atomic Energy Agency (JAEA) and Chinese Academy of Sciences (CAS).

## 2. VE in Mont Terri URL

### 2.1. Short description

The Mont Terri URL is located near a security gallery of a motorway tunnel in northern Switzerland (Bossart and Nussbaum, 2007). It is at a depth of about 400 m in Opalinus clay, which is a stiff layered Mesozoic clay of marine origin. Initially opened to experiments in 1996, a new gallery was excavated in 1998, followed by a 1.3 m diameter micro-tunnel in early 1999. A 10 m long section of this micro-tunnel was used for the VE as shown in Fig. 1.

After excavation, the micro-tunnel was left without atmospheric control for approximately 3.4 years. After this period, doors were installed in order to create a section of 10 m in length, where the atmospheric conditions could be controlled through a prescribed air inflow rate and inflowing relative humidity (RH) (Fig. 2). Appropriate monitoring inside the tunnel and rock wall enabled accurate picture of the conditions in and around the tunnel to be established (Garitte et al., 2013). The micro-tunnel has been intensively instrumented with RH sensors, pore pressure sensors and displacements sensors. Two water pans have been installed in order

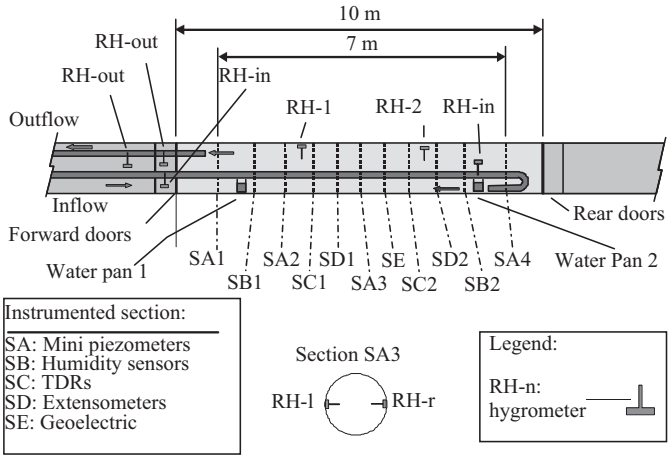


**Fig. 2.** Controlled ventilation section in the micro-tunnel, and relative humidity measurement locations.

to record the evolution of water mass loss due to the ventilation. Their locations are indicated in Fig. 2. The variation of the RH with time, at different points along the micro-tunnel, is shown in Fig. 3.

The micro-tunnel was subjected to two wetting-drying cycles. The first cycle lasted from 8 July 2002 to 29 January 2004 (Phase 1). Initially 100% RH inflowing air wetted the micro-tunnel and then provoked a desaturation period, 2% RH air was applied to the tunnel inflow. This first cycle was then followed by a further cycle, and a final resaturation period which continued until 2010 (Phase 2), although data were only available until April 2007. The corresponding total sequence of prescribed RH is illustrated in Fig. 3 (curve RH-in, in red).

### 2.2. Summary of hydro-mechanical behaviour

The HM response of the system was described in detail by Garitte et al. (2013). However, in general terms the evolution of the system can be described as follows, repeated from Bond et al. (2013):

(1) A known rate of air with a defined RH is input into the sealed section of the tunnel.
(2) Interaction between the water vapour in the tunnel and the unlined tunnel host-rock results in vapour exchange between the tunnel and the host-rock. Evaporation of liquid water from the tunnel surface may also occur depending on local tunnel RH.

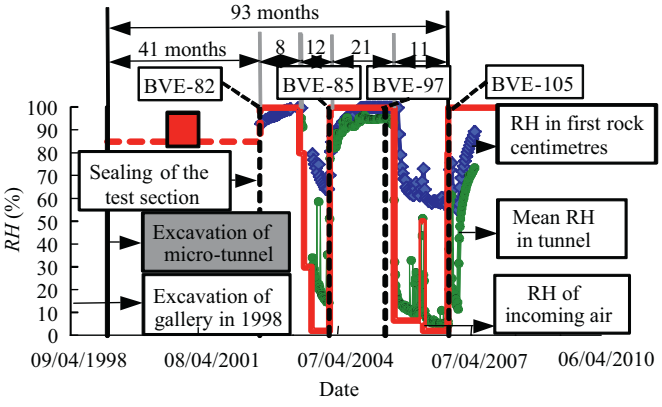


**Fig. 3.** Relative humidity history of the test section from Garitte et al. (2013).

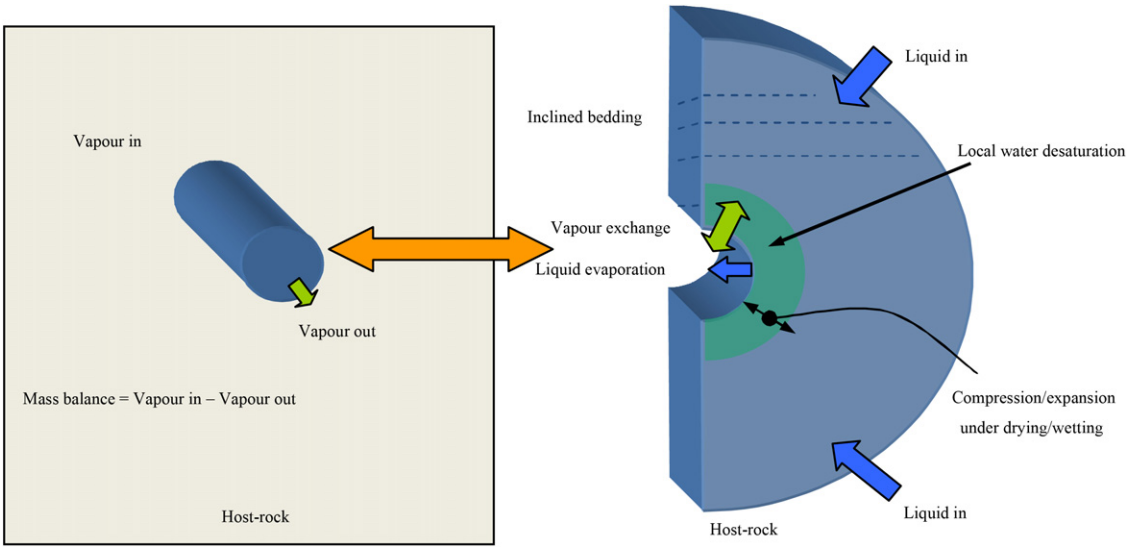


**Fig. 4.** Schematic conceptual model of the hydro-mechanical system.

(3) Water vapour leaves the tunnel via a measurement gauge for RH and air rate. The difference between points 1 and 3 above constitutes the tunnel water balance.
(4) Loss of water from the host-rock to the tunnel as vapour causes a reduction in water pressure and saturation as air invades the formation from the host-rock.
(5) The reduction in liquid pressure and RH around the tunnel causes liquid water and water vapour (where present) to migrate towards the tunnel.
(6) Desaturation and reduction in fluid pressure cause reduction in pore volume and limited shrinkage of some of the rock skeleton, causing a local net drop in volume of the host-rock.
(7) The volume change of the host-rock causes localised stress changes and coupling with the hydraulic evolution through a reduction in porosity, which creates a coupling with fluid pressures and intrinsic permeability.

The processes described above are illustrated in Fig. 4. The dominant process models and those which have been represented by the modelling teams in DECOVALEX are therefore vapour diffusion in and advection by, air in porous media and engineered volumes; viscous dominated multi-phase flow of air and water in porous media; and poro-mechanical deformation of the host-rock.

## 3. Opalinus clay drying test

This complimentary experiment to the main VE has been discussed in some detail by Garitte et al. (2010, 2013), Floría et al. (2002) and complemented by supporting data from Muñoz et al. (2003). The experiment is illustrated schematically in Fig. 5, however, a brief summary follows. The drying test was a well constrained laboratory experiment where three cylindrical samples of Opalinus clay (101 mm in radius and 254 mm in height) were placed in a controlled drying chamber along with an evaporation pan, axial direction oriented vertically. Chamber RH and airflow were monitored continuously throughout the 142-day experiment. The samples were covered such that the upper circular surface only could lose water through evaporation. The samples and evaporation pan were also weighed continuously such that water loss could be monitored. Samples were removed and dissected at 21, 99 and 142 days such that the water content profile vertically from the evaporation surface could be monitored.

From this combination of data, a continuous record of water loss for each sample as a function of the chamber conditions could be established, along with the sample water content profiles at 21, 99 and 142 days.

As discussed in Garitte et al. (2013), this experiment was used as a precursor modelling exercise by DECOVALEX in order to reduce uncertainty and build confidence in codes, process models and hydraulic parameterisation before attempting the full VE. The experiment also provided a useful role in understanding the possibilities for upscaling processes and parameters from the laboratory scale to the field scale.

## 4. Treatment of the surface condition

Successful treatment of the surface condition in both the drying test and the VE is manifestly important in ensuring a good representation of the interface between the air filled void (tunnel or drying chamber) and the porous medium. The drying test represented a controlled set of data where options were employed for representing these conditions before attempting the more complex VE.

### 4.1. Approaches

Two general approaches for defining the liquid water boundary condition were utilised based on the available data and conceptual understanding of the experiments. The first used Kelvin's law to define an equivalent water pressure ($p_l$) at the surface, representative of the air RH in the tunnel or drying chamber:

$$p_l = p_a - \frac{RT}{M_w}\rho_l \ln(RH) \quad (1)$$

where $p_a$ is the air pressure (Pa), $R$ is the ideal gas constant (J mol$^{-1}$ K$^{-1}$), $T$ is the temperature (K), $M_w$ is the molar mass of water (kg/mol), $\rho_l$ is the density of water (kg/m$^3$), and RH is the relative humidity in the air expressed as a fraction (–). This boundary condition is best described as a time-variant Dirichlet condition, and will be referred to as the "pressure" variant in the remainder of this paper.

The second used an empirical relationship which correlated the observed open pan evaporation rate in each experiment ($F_f(RH)$, kg m$^{-2}$ s$^{-1}$), versus the RH in tunnel or drying chamber. For each

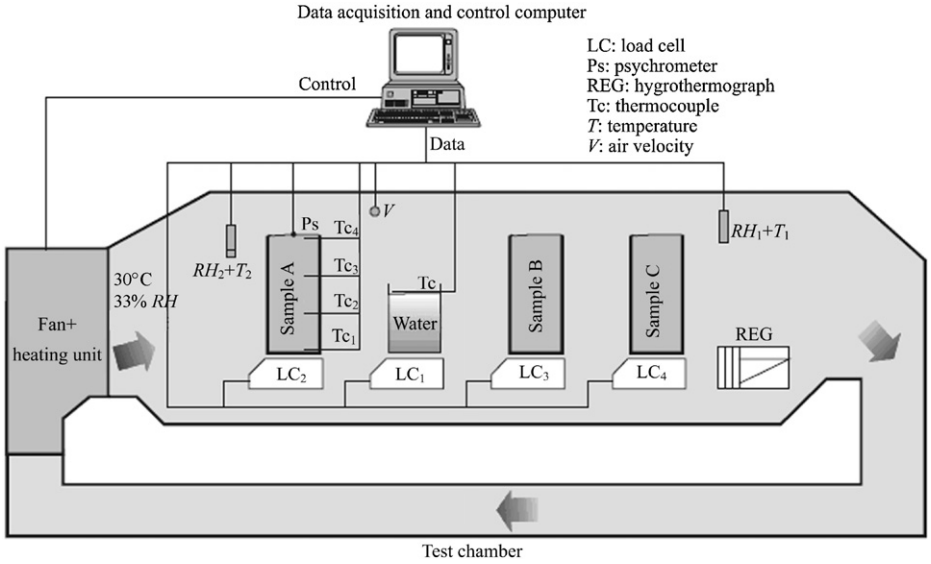


**Fig. 5.** Schematic illustration of the drying test, modified from Floría et al. (2002).

experiment, a simple functional relationship was derived between the two observations. Note that changes in air circulation rate, which might be reasonably assumed to affect the local rate of evaporation, were neglected under the assumption that mixing of the air was relatively rapid. The function was then scaled by the fractional effective area of the free liquid water assumed to be presented at the rock surface. The assumption was that this fractional effective area could be described by the product of the porosity ($\theta$) and water saturation ($S_w$) at the top of the sample. Hence the effective water loss flux could be described as

$$F_e = \theta S_w X F_f(RH) \tag{2}$$

where $X$ is a penalty coefficient (–) that enables additional scaling of the flux based on additional factors that are not covered in the fractional area term. Clearly, this formulation requires a good estimate of the saturation at the evaporation surface to function adequately. Dependent on the model formulation, there are a number of approaches that can be adopted to achieve this, the most obvious being a high degree of spatial discretisation up to the evaporation surface. In mathematical terms, this type of condition is a weak form of "mixed" condition, whereby a time-variant Neumann flux ($F_f(RH)$) is scaled by properties internal to the model. This boundary condition is best described as a time-variant Neumann condition, and will be referred to as the "flux" variant in the remainder of this paper.

Both of these models assume that mixing in the tunnel is relatively rapid compared with the loss from the porous medium, and hence there is no need to consider any boundary layer effects.

For numerical formulations where the water vapour was considered explicitly (Garitte et al., 2013; Zhang et al., 2013), the surface boundary condition for vapour was simply water vapour diffusion continuity equation using the RH in the tunnel or drying chamber to define the water vapour density as a time-variant Dirichlet condition, thus we have

$$\rho_v = 10^{-3} \exp\left(a - \frac{b}{T}\right) RH \tag{3}$$

where $\rho_v$ is the vapour density (kg/m$^3$), $a$ is an empirical constant (−19.891), and $b$ is an empirical constant (4975.9 K) (Rutqvist et al., 1999).

### 4.2. Comparison for the drying test

The relative behaviours of the two approaches were investigated by a number of DECOVALEX participants for the drying test. As a representative example of the drying test, the model developed using QPAC (Maul et al., 2010) will be discussed here in detail.

The drying test model consisted of a one-dimensional (1D) cylindrical grid discretised in the axial (vertical) direction using 12 finite volume compartments (Fig. 6), a discretisation which has been shown to be numerically sufficient for accurate

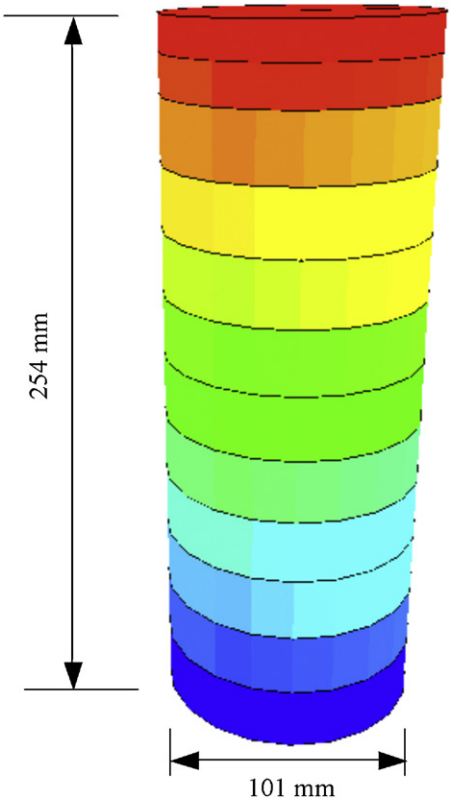


**Fig. 6.** Drying test QPAC grid. Volumes are coloured by centroid elevation.

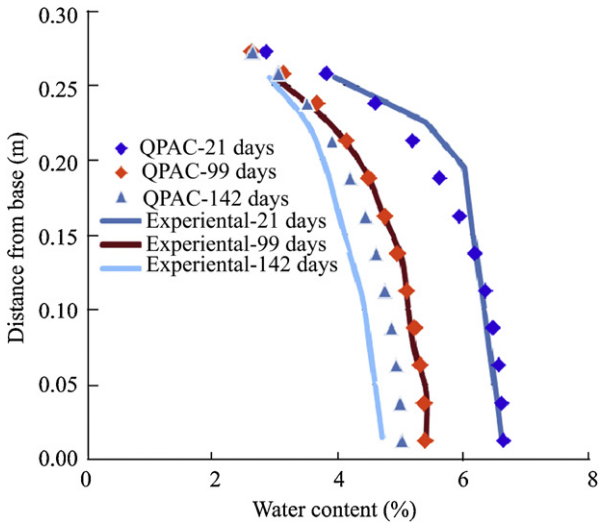


**Fig. 7.** Comparison of calculated water contents for the three samples in the drying test versus the calculated QPAC results using the pressure based upper boundary condition.

representation of this case. All boundaries were set as non-flow, except for the top boundary where one of the two boundary conditions described in the previous section could be applied. Full multi-phase flow, incorporating water, air and water vapour, was employed and the constitutive equations for gases (g consisting of $j$ gas phases) and water (w) overall flowing phases ($i$) are given below:

$$\left.\begin{aligned} &\frac{\partial}{\partial t}(\theta\rho_i S_i) = -\nabla\cdot(\rho_i \boldsymbol{u}_i) + q_i \\ &\boldsymbol{u}_i = -\frac{\boldsymbol{k}_i}{\mu_i}\nabla(p_i + \rho_i g z) \\ &\boldsymbol{k}_i = k_{r,i} S_i \boldsymbol{k} \\ &\psi = p_{g_j} - p_w \end{aligned}\right\} \quad (4)$$

where subscript $i$ denotes the phase, $\rho_i$ is the density (kg/m$^3$), $\boldsymbol{u}_i$ is the volumetric flux (m/s), $q_i$ is an external mass source (kg/s), $S_i$ is the saturation (–), $\boldsymbol{k}_i$ is the intrinsic permeability (m$^2$), $k_{r,i}$ is the relative permeability (–), $\psi$ is the capillary pressure (Pa), and $z$ is the elevation.

The vapour mass fluxes (kg s$^{-1}$ m$^{-2}$) for diffusion and advection in bulk gas are

$$\left.\begin{aligned} &u_{v,\mathrm{diff}} = -D_v S_g \nabla\rho_v \\ &u_{v,\mathrm{adv}} = u_g \rho_v \end{aligned}\right\} \quad (5)$$

where $D_v$ is the effective diffusivity of water vapour (m$^2$/s), which is assumed to be a function of bulk gas saturation. For this case, the effective vapour diffusivity was assumed to be the gas saturated effective vapour diffusivity multiplied by the total gas saturation.

The reference model used the pressure boundary condition variant and produced results that were a good fit to the observed water contents, taking into account heterogeneity between the samples (Fig. 7). The parameterisation is given in Table 1.

The equivalent outputs for the calculation using the specified flux upper boundary condition are shown in Fig. 8 using a penalty factor $X$ (Eq. (2)) of 1 and an implied free evaporation rate at zero RH ($F_f(RH=0)$) of 1.1 g d$^{-1}$ cm$^{-2}$, reducing linearly to zero at a RH of 100%. While there are some small differences, the basic result is equivalent. Simple parametric sensitivity studies showed that

**Table 1**
Hydraulic parameterisation for the QPAC model of the drying test.

| Reference porosity $\theta_0$ | Relative permeability air $k_{r,A}$ | Relative permeability water $k_{r,w}$ | Intrinsic permeability $k$ (m$^2$) | Reference vapour diffusivity $D_v$ (m$^2$/s) | Suction pressure $\Psi$ (MPa) | Initial water saturation | Dry grain density $\rho_m$ (kg/m$^3$) |
|---|---|---|---|---|---|---|---|
| 0.16 | 1 | $S_{wr}^{(1/2)}[1-(1-S_{wr}^{(1/\lambda)})^{\lambda}]^2$ where $S_{wr}$ is the reduced saturation and $\lambda$ (=0.35) is a fitting parameter | $k_0[\theta^3/(1-\theta)^2]\times[(1-\theta_0)^2/(\theta_0)^3]$ where $k_0 = 9.375\times10^{-20}$ m$^2$ | $2.5\times10^{-6}$ | Determined by constraint solution to: $0 = S_{wr}(1-F_{vapour}) - \{1+(\Psi/P_0)^{1/(1-\lambda)}\}^{-\lambda}\cdot[1-(1-\psi/P_s)^{\lambda_s}]$ where $P_0 = 3.9$ MPa $\lambda = -0.128$ $P_s = 700$ MPa $\lambda_s = -2.73$ | 0.999 | 2700 |

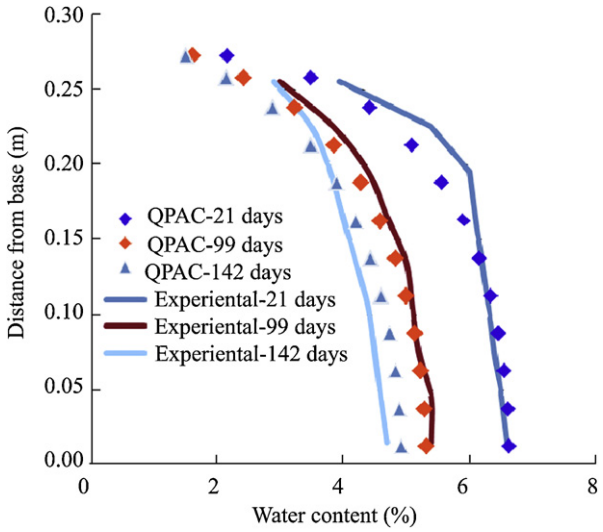


**Fig. 8.** Comparison of calculated water contents for the three samples in the drying test versus the calculated QPAC results using the flux based upper boundary condition.

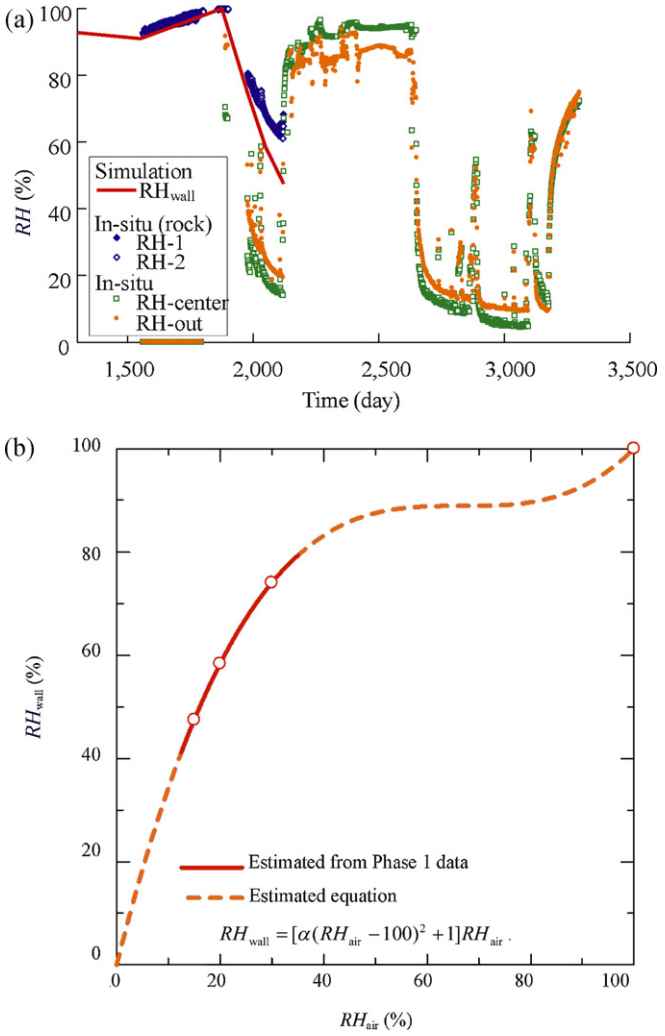


**Fig. 9.** (a) Estimated tunnel wall relative humidity from early-time simulations and (b) the resultant correlation between average tunnel relative humidity and wall relative humidity.

functionally identical results can be produced with only minor adjustments to the parameterisation of intrinsic permeability, relative permeability or vapour diffusivity, all of which are well within the accepted bounds of data uncertainty for this case. Unfortunately, required brevity prohibits a full discussion of this parameter space search.

A key numerical point is that, in order for the flux version of the case to work adequately, estimation of the water saturation at the upper surface of the sample needs to be accurate. Because a finite volume approximation was adopted in this case, primary variables are calculated at compartment centres; hence no water saturation was calculated at the boundary. In this case, this was addressed through estimating a boundary water saturation using the inferred water saturation profile through the upper half of the model via an automatic, dynamic high-order polynomial fit, and using this directly in the water flux calculation.

The required parameter changes to make one solution equivalent to the other are sufficiently small relative to other uncertainties, that the difference between the two boundary condition approaches is effectively negligible for the drying experiment. However, it is recognised that this congruence of approaches may not generally be true, and caution should be adopted in different environments.

Depending on the assumptions made, this was not the case in the full VE. The differences that can come about due to differing assumptions regarding the behaviour of the tunnel and the meaning of the data are illustrated in Section 5 as they are intrinsically linked to the treatment of the tunnel.

## 5. Treatment of the VE tunnel

A key assumption in the interpretation of this experiment was that the tunnel was part of the experiment, and as such it was strongly preferable for the RH to be dynamically calculated on the basis of the interactions between the applied tunnel RH, air flow rate and the interaction with the rock mass.

Three general classes of approach were developed by the DECOVALEX participants to address the dynamic representation of the tunnel:

(1) Empirical, correlated model.
(2) Abstracted model, considering a simplified physical model of the tunnel system.
(3) Detailed model, where dynamic physical models of the air and water vapour in the tunnel are considered.

The approach and selected results for each will be considered in turn, noting that approach 1 is the manner in which the drying test was treated. It should be noted that, as discussed in Garitte et al. (2013), good agreement was achieved between the teams in terms of their HM analysis, and as such it is possible to use the results obtained by different teams exploring different aspects of the problem in a holistic to derive general conclusions for this case.

### 5.1. Empirical and correlated models

The simplest approach adopted was to examine the available data regarding the tunnel average RH versus the expected RH at the tunnel wall. This approach is necessary as it is clear that the magnitude of this variation will strongly control the water loss from the tunnel wall. Given the likely vapour dominated diffusive nature of the tunnel (Section 3), as could be reasonably expected, a good

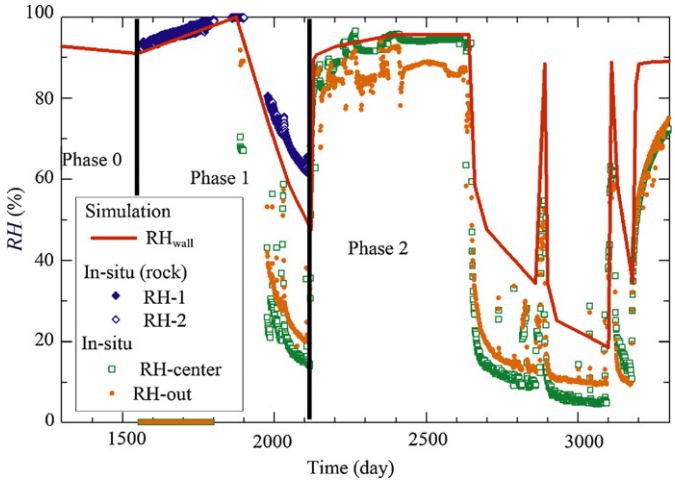


**Fig. 10.** Extrapolated tunnel wall relative humidity for Phases 0, 1 and 2.

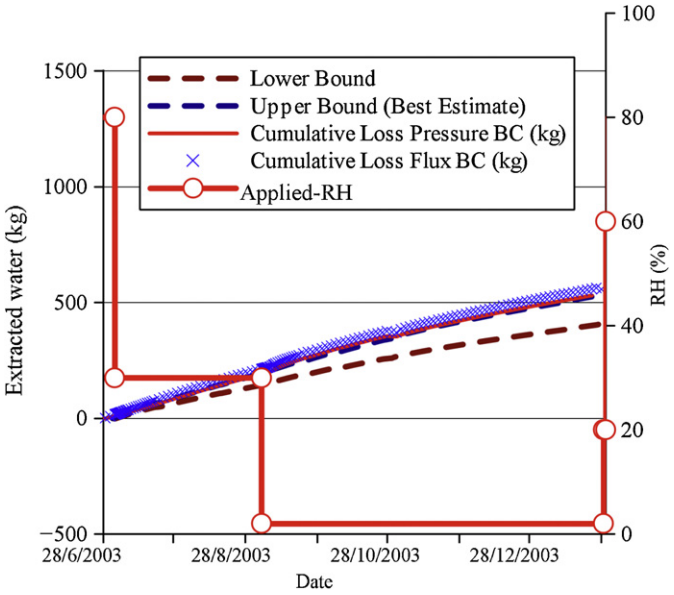


**Fig. 11.** Calculated mass balance versus experimental data for the CEA model, comparing the "pressure" and "flux" based approach for the tunnel liquid water boundary condition.

correlation can be obtained between these properties as shown in Fig. 9 and those developed by the JAEA team.

This functional form could then be used in place of the average tunnel RH to act as the boundary condition on the tunnel wall using information on tunnel average RH. This was the case during the second wetting/drying phase (Phase 2) and the resultant tunnel condition is shown in Fig. 10.

This approach enables the modeller to better estimate wall conditions from average tunnel conditions, but it is clearly a highly specialised model. This approach is calibrated against this particular experiment and does not allow forward prediction given only information on the inflowing tunnel RH and the air flow rates.

Using a very similar approach to understanding the variation of RH at the tunnel wall versus the humidity in the tunnel as a whole, the CEA team modified their case to move from the pressure-based boundary for liquid water to the flux-based method, and thus compared the relative consistency between the two boundary modelling approaches. A full discussion of the CEA model is given in Millard et al. (2013). Fig. 11 illustrates the difference in calculated mass balance during the Phase 1 period, clearly illustrating that the "pressure" and "flux" approaches given very similar responses. The pressure and RH data show a similarly coherent response, a behaviour that is consistent with the observations for the drying test calculations.

### 5.2. Abstracted approach

In order to give a model of the tunnel that could be used in a more predictive manner, simplified models of the tunnel itself were constructed by a number of teams. This class of approach considers the distribution of water vapour in the tunnel explicitly, hence allowing for a simple model of the migration of water vapour in the tunnel itself. Such a model allows the boundary conditions of the model to be defined as the inflow and outflow of air from the tunnel, rather than being the tunnel wall. The key simplification in these approaches is that the behaviour of the air is applied as a model input rather than being calculated.

The model using QPAC (Maul et al., 2010) is given here as the principal example which utilises the general conceptual model that has been described in Sections 2 and 3. A numerical approach was developed that would enable the general processes of vapour migration to be modelled, given a range of different assumptions regarding the flow patterns of the air in the tunnel. In this way, the impact of conceptual uncertainty on the behaviour of the air (and its consequential impact on the vapour) could be understood in terms of the measurements available.

#### 5.2.1. Numerical model – Opalinus clay

The QPAC implementation considered two sub-systems: the tunnel and the porous medium (Opalinus clay). The porous medium model considers coupled HM processes using the same multi-phase flow formulation discussed in Section 4. The mechanical component used in this example was a poro-elastic formulation with effective stress coupling through a simple Bishop effective stress model (Bishop, 1959). Changes in porosity through net volumetric strain changes also gave rise to permeability changes through the Kozensky relationship (Tables 1 and 2), which has been also applied to clay systems, while it is traditionally applied to open soils and sands. System discretisation in the porous media was using a reclined, cylindrical grid which could be discretised arbitrarily in 1D, 2D or 3D. In all cases, the radial direction was always fully discretised, using 45 compartments in an approximately geometrically increasing grid size from the tunnel wall. In the angular direction, half of the tunnel system is represented while the full tunnel length is selected for the thickness of the cylindrical compartments. Using these dimensions enables easy comparison with the water balance data and allows the angular and tunnel length directions to be discretised with only very minor changes to the input. Various analyses, not discussed further here, established that this grid refinement was appropriate, and that a 1D cylindrical representation was appropriate in most cases, given the available data. Such issues were discussed in more detail in Garitte et al. (2013) and Zhang et al. (2013). The input parameters, derived from the drying test and subsequently calibrated using the observed tunnel RH information, are provided in Table 2 and an illustration of the model domain and grid was presented in Fig. 12. The default QPAC model used the "flux" version of the surface condition for describing the liquid water interaction between the Opalinus clay and the tunnel.

**Table 2**
Hydro-mechanical parameterisation for the QPAC model of the ventilation experiment.

| Acceleration due to gravity, $g$ (m/s$^2$) | Young's modulus (clay), $E$ (GPa) | Poisson's ratio (clay), $\nu$ | Viscosity (clay), $\mu$ (Pa s) | Failure mode (clay) | Reference porosity (clay), $\theta_0$ |
|---|---|---|---|---|---|
| 9.812 | 1 | 0.3 | 0 (creep disabled) | None – elastic only | 0.165 |
| **Initial deviatoric stress (atmosphere (bar))** | **Initial water pressure (atmosphere (bar))** | **Initial temperature (°C)** | **Reference water density (kg m$^{-3}$)** | **Reference water pressure (atmosphere (bar))** | **Relative permeability air $k_{r,A}$** |
| 0 (all directions) | Hydrostatic | 15 | 1000 | 1 | 1 |

| Relative permeability water, $k_{r,w}$ | Intrinsic permeability, $k$ | Reference vapour diffusivity, $D_v$ (m$^2$) | Suction pressure, $\Psi$ (m$^2$ s$^{-1}$) | Initial water saturation (MPa) |
|---|---|---|---|---|
| $S_{wr}^{(1/2)}[1-(1-S_{wr}^{(1/\lambda)})^{\lambda}]^2$ where $S_{wr}$ is the reduced saturation and $\lambda$ is a fitting parameter = 0.3 | $k_0[\theta^3/(1-\theta)^2]\times[(1-\theta_0)^2/(\theta_0)^3]$ where $k_0 = 1.125\times10^{-19}$ m$^2$ | $2.50\times10^6$ | Determined by constraint solution to: $0 = S_{wr} - [1+(\psi/P_0)^{1/(1-\lambda)}]^{-\lambda}(1-\psi/P_s)]^{\lambda_s}$ where $P_0$ = 3.9 MPa, $\lambda = -0.08$, $P_s$ = 700 MPa, $\lambda_s$ = 2.73 | 0.99999 |

| Dry grain density, $\rho_m$ (kg/m$^3$) | Effective pore pressure (for calculating effective stress) (MPa) | Phase 0: applied RH | Phase 0: applied air flow rate (m$^3$/h) | Tunnel free air diffusivity (m$^2$/s) | Maximum evaporation rate $F_f$ (RH = 0) (g/(d cm$^2$)) |
|---|---|---|---|---|---|
| 2700 | $P_w S_w^n + P_{air}(1-S_w^n)$ $n$ = 1 | 0.6 | 30 | Axial: $2.50\times10^{-5}$ Radial: $2.50\times10^{-4}$ (included artificially enhanced turbulent mixing factor) | 0.073, $F_f$ reduces linearly to zero at RH = 100% |

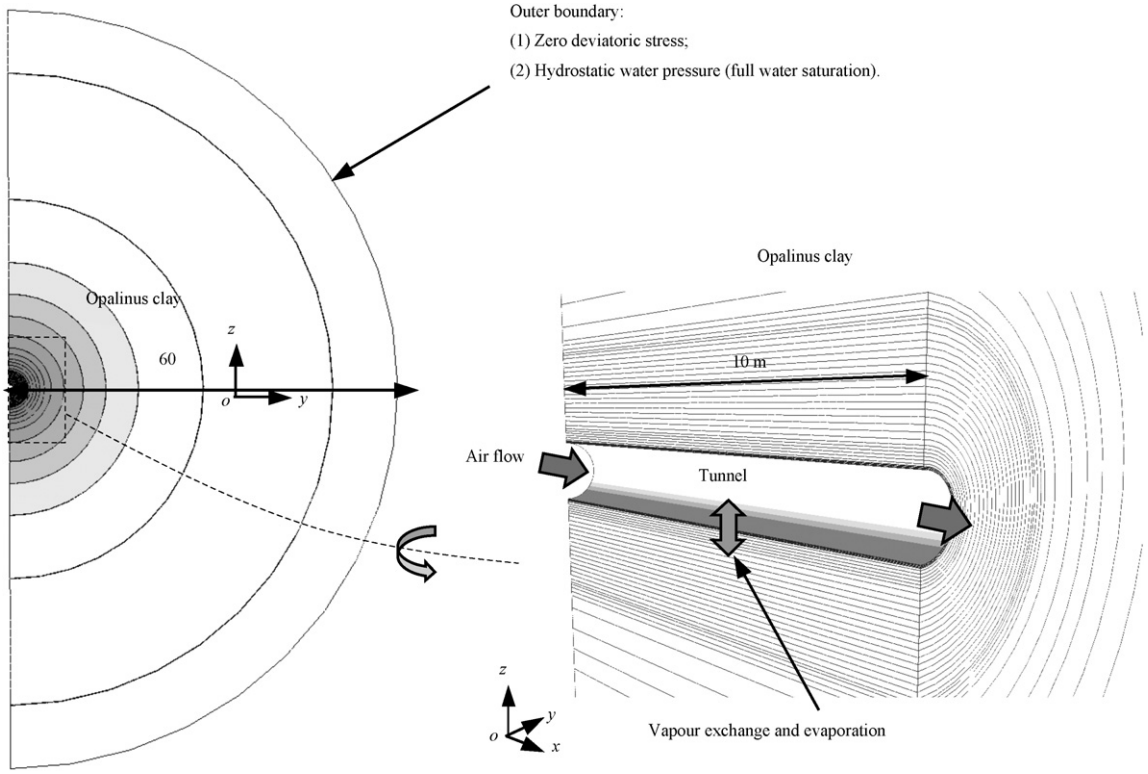


**Fig. 12.** Porous medium grid geometry for the QPAC calculations. 1D cylindrical compartments are coloured by radius and shown for the Opalinus clay only. The 1D cylindrical compartments have a defined thickness (along the axis of the tunnel) of 10 m, and hence represents an average behaviour along the length of the tunnel.

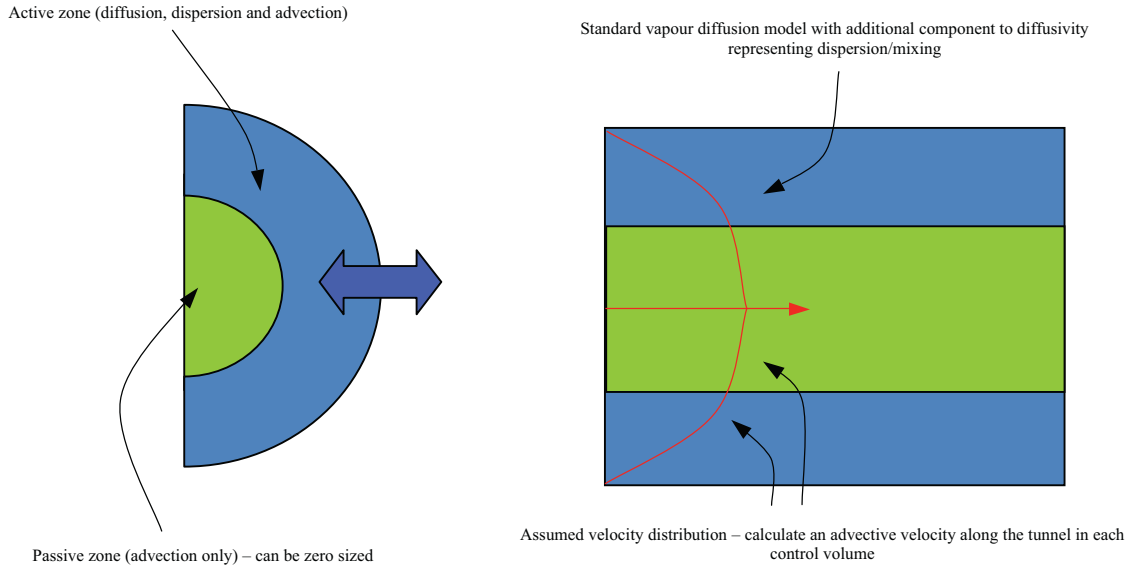


**Fig. 13.** Schematic illustration of the conceptual model for QPAC abstracted tunnel model.

*5.2.2. Numerical model – tunnel*

The tunnel model was designed to accommodate the features induced by the interaction between air flow and water vapour that might be reasonably expected to exist. These features were:

(1) An "active" zone and a "passive" zone in the radial direction; the active zone interacting with the tunnel wall and the passive zone not doing so (and hence not interacting with the active zone), only transporting the vapour associated with the injected air. The passive zone may be zero-sized.
(2) Water vapour migration in the active zone is diffusive both radially and axially with an advective component along the axis of the tunnel caused by the local air velocity.
(3) Any impact of turbulent mixing of the air can be considered through enhanced radial diffusion, acting to more quickly equilibrate water vapour radially in the tunnel.
(4) A velocity distribution for air parallel to the tunnel axis may be defined locally.
(5) Interaction between the outer tunnel and the porous media through evaporation of liquid water and vapour diffusion.

The primary objective of including such features was to allow the impact of the uncertainty in the above conceptual and parametric uncertainty to be explored in a single model, and hence to deliver a more predictive model with a good understanding of the likely errors that might be produced from the assumptions on the detailed air flow. This model is illustrated in Fig. 13.

The numerical implementation is extremely simple, consisting of a mass balance of water vapour in each compartment and migration through diffusion in air and advection by air using Eq. (5). Discretisation was set to be consistent with the axial and angular discretisation in the porous medium sub-system. Radial discretisation was 6 compartments with the outer compartment 5 cm in depth and the remainder uniformly 10 cm in thickness to the centre of the tunnel.

Interaction between the tunnel and the porous media was through local coupling of the boundary equations for evaporation of water (Eq. (2)) and continuity of water vapour (Eq. (3)). Coupling was achieved through using the RH and water vapour density calculated in tunnel compartments adjacent to the tunnel wall to define the fluxes in the boundary equations. The water and water vapour fluxes are then conserved between the two sub-systems. It should be noted that the coupling mechanism employed used a fully implicit scheme such that both the tunnel and porous media HM equations were solved as a single set of equations, rather than using some form of operator splitting or sequential coupling method. In this context, the implementation of Eqs. (2) and (3) is no longer boundary conditions, but internal continuity equations of a different form to those used in the sub-systems (either side of the connection).

Boundary conditions on the tunnel model consist of simple advective flows of water vapour at the inflow and outflow ends. Consistent with the formulation in the tunnel model, the advective flows on the boundaries are upwinded, hence the inflow of water vapour is the product of the experimentally applied vapour density (from RH) and the air flow rate. Similarly, at the outflow end of the tunnel, the rate loss of vapour is given by the product of the calculated water vapour density in the upwind adjacent compartment to the boundary and the air flow rate.

Given that the reference model used a simple 1D discretisation, the whole 10 m length of the tunnel and circumference was represented using a single compartment. Investigations on the impact of the tunnel and host rock being discretised along the length of the tunnel are discussed in the following sections.

*5.2.3. Calibration and reference results*

A range of sensitivity analyses were conducted on the parameterisation of vapour migration and air movement in the tunnel. The first major conclusion was that in order for the observations on tunnel inflow/outflow mass balance and interaction with the host-rock to be consistent with the known water content data in the Opalinus clay, the whole tunnel had to be contributing significantly, i.e. there could be no "passive zone". Such an observation is consistent with the small tunnel radius and relatively slow airflow rates through the tunnel. The second major conclusion was that there was relatively little sensitivity to the radial velocity distribution and the inclusion or exclusion of enhanced radial mixing (turbulence) in the model.

The comparison between the observed average RH in the tunnel and the calculated values (see Fig. 14) are extremely close throughout the experiment. The results clearly show very similar magnitudes and transient behaviours even during the rapid

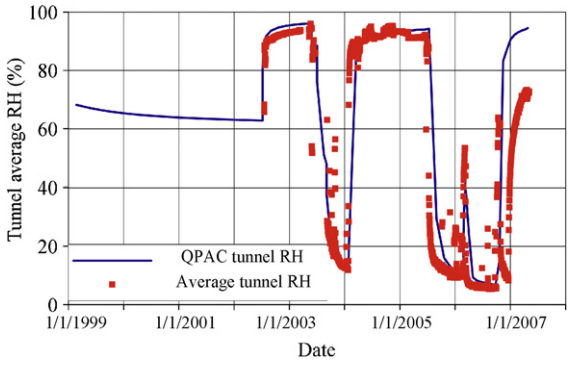


**Fig. 14.** Comparison between the calculated and observed relative humidity of air in the experimental tunnel.

changes in 2006. There was clearly a deviation between the curves at the end of 2006 and during 2007, but this appears to come about due to erroneous or missing data. Similarly, good results were obtained for total mass balance (Fig. 15), RH, water content in the rock mass and rockmass dimensional change with time (Fig. 16) (Garitte et al., 2013; Zhang et al., 2013). The bulk water mass balance shows the calculated results tracking the experimental estimates well with time. It is noted however that while the model shows similar drying rates during Phases 1 and 2, the experimental data may suggest a slower response during Phase 2, although the deviation is within the bounds of data uncertainty, and hence cannot be positively isolated as a trend. If presented, this trend might be indicative of a bulk reduction in intrinsic permeability with time, potentially associated with healing of rock damage through creep.

The modelled mechanical evolution versus observations for Phase 1 is illustrated in Fig. 16. The experimental data showed considerable variation, although not apparently structured variation, and hence for the 1D case used here, comparison is made versus the data of B47, which exhibited a reasonable median behaviour of the available data. The model results show the initial expansion of the rock mass through tunnel construction, and then progressive contraction through Phase 0 (for which we have no data) as drying takes place. The wetting-drying cycle during Phase 1 is well

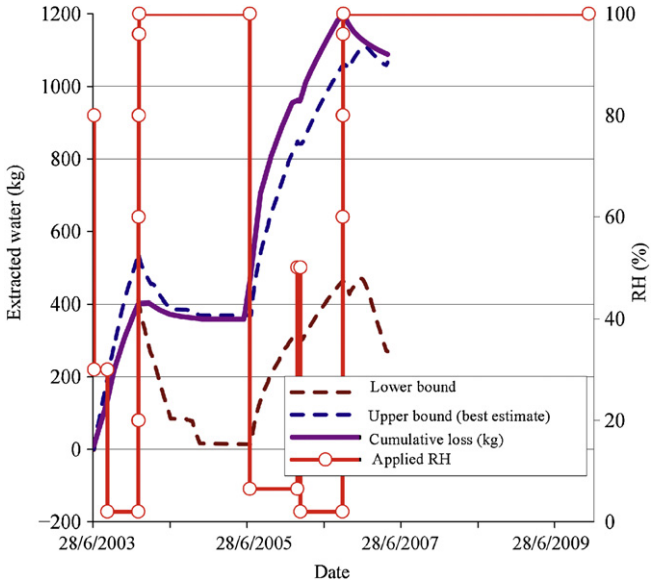


**Fig. 15.** Comparison between the calculated and observed water balance in the ventilation experiment tunnel.

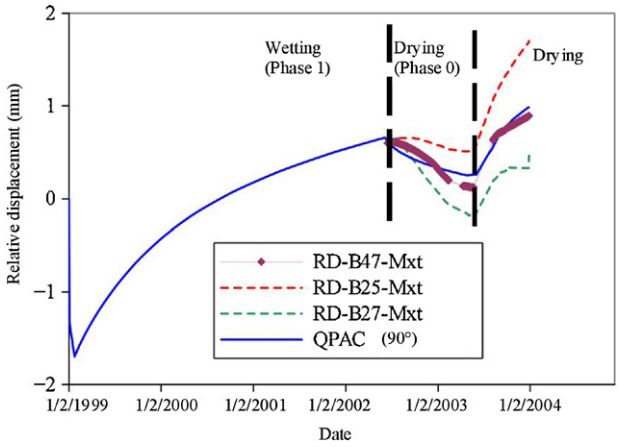


**Fig. 16.** Comparison between the calculated and observed relative displacements during Phases 0 and 1.

captured in terms of the expansion and contraction of the extensiometers. It should be noted that the elastic modulus used for the model is towards the lower end of expected intact rock values, and this may be indicative of the effects of damage, or alternatively, that the poro-elastic model needs to subsume other processes, such as clay swelling, which will exaggerate dimensional change.

### 5.2.4. *Pressure-based surface condition*

To test the conclusion of Section 4 that the sensitivity of the model result is small with respect to the choice of the type of surface boundary applied, the model described in the previous section was adjusted to use the pressure-based surface formulation. The result was quite striking. Early-time results were very similar, consistent with the CEA results in Section 4. However, during the major drying component of Phase 2, the drying effect is magnified, resulting in a peak loss of 1300 kg of water (compare with about 1100 kg shown in Fig. 15. It appears that under strong drying conditions, the pressure formulation was exerting a much greater control.

However, resolving this discrepancy could be readily achieved through one of two methods either:

(1) Scaling intrinsic permeability by a factor of 3/4 and changing the λ factor in the relative permeability formulation (Table 2) from 0.35 to 0.3;
(2) Eliminating the enhanced lateral turbulent mixing in the tunnel to induce vapour density gradients across the tunnel radius (Figs. 17 and 18).

Figs. 17 and 18 show that the deviation of the wall RH from the average tunnel RH is quite small, even under strongly drying conditions. Neither change is especially large and is covered by the conceptual and parameter uncertainty inherent in the data model.

The conclusion must be that for the VE formulation, the pressure-based approach for the surface condition is more sensitive to the assumptions, regarding the distribution of water vapour in the tunnel than the flux-based approach. However, small changes in the parameterisation of the porous media can overcome this sensitivity relative to the flux-based formulation. Unless additional data can constrain the characteristics of the system further from this analysis, it must be concluded that the assumptions of the details of the behaviour of the tunnel with regard to water vapour distribution are of secondary importance in this system.

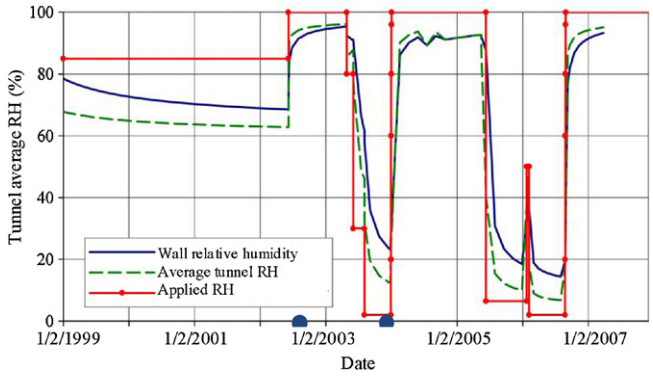


**Fig. 17.** Comparison between the average and wall relative humidity calculated in the QPAC tunnel model when using the pressure formulation for the surface boundary and no enhanced radial mixing. The times for the relative humidity plots in the tunnel shown in this figure are highlighted by spots on the *x*-axis.

### 5.2.5. *Discretisation along the tunnel axis*

In order to test the assumption, treating the tunnel and Opalinus clay with a single compartment in the tunnel axial direction was appropriate to understand the modelled variation of RH along the axis of the tunnel, and the reference case was divided into five compartments axially. The average RH at each distance along the axis of the tunnel and the results are plotted together with the applied RH. In addition, comparison was made between the estimated mass balance from the outflowing water vapour and that produced from the 1D calculation.

The computed mass balance is visually indistinguishable from Fig. 15, and as such is not discussed further. The variation along the tunnel is shown in Fig. 19. The difference between the upstream and downstream relative humidities is of the order of 10–15% under strongly drying conditions, which is similar to the variation along the tunnel shown in the experimental observations (Fig. 20). The model shows slightly less variation than observed by the inflow and outflow data, especially at early times. But this can be understood by noting that the evaluation points in the model are 1 m away from the ends of the tunnel, and hence the full variation cannot be captured.

Given the similarity in results between the 1D and 2D cases, the model reproduces the observed variation in RH along the axis of the tunnel. It appears that this abstracted approach gives a good representation of the tunnel for understanding the hydraulic mass balance of the system, and as a more complete "boundary" to the porous medium HM model.

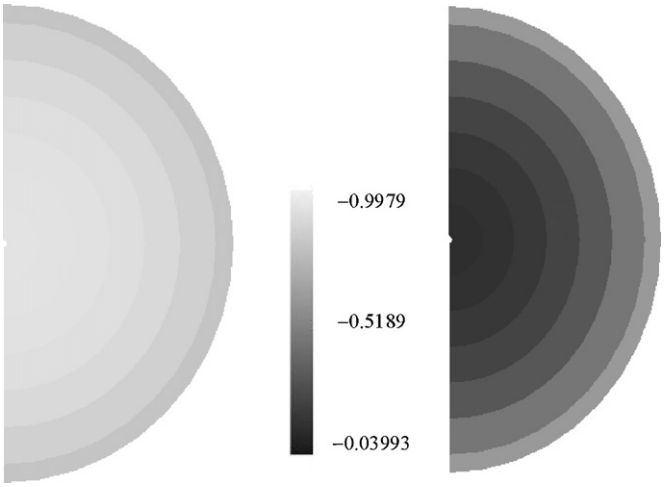


**Fig. 18.** Relative humidity across the tunnel (shown as a half model) on 8 July 2002 (left) and 1 November 2003 (right), showing the relative small amount of relative humidity change across the tunnel with no enhanced radial water vapour mixing.

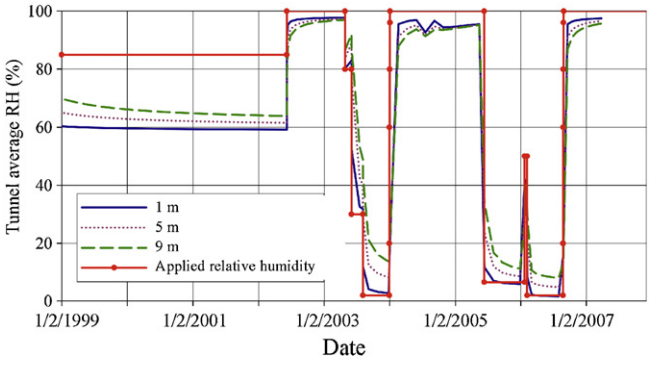


**Fig. 19.** Plot of average relative humidity across the tunnel with different distances along the tunnel axis from the air inlet, at 1 m, 5 m and 9 m.

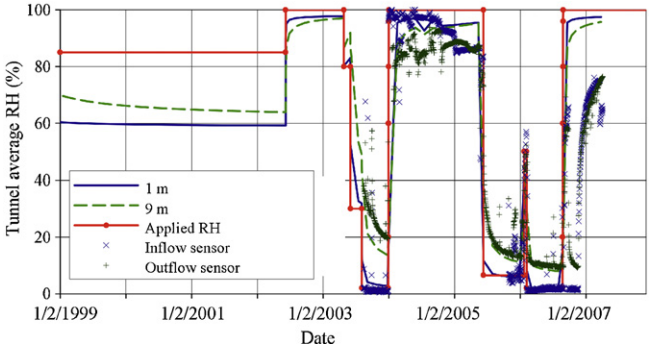


**Fig. 20.** Plot of average relative humidity along the tunnel at 1 m and 9 m from the air injection, in comparison with the inflow and outflow relative humidity data.

## 5.3. *Detailed approach*

The final approach involved making a more complete physical assessment of the system, which was adopted by CAS. A continuum fluid dynamics (CFD) analysis was adopted whereby the details of the injection and extraction of air into a simplified representation of the tunnel to calculate an air velocity distribution were presented. Initial results showed that while the air flow was dominantly laminar, the flow pattern was quite sensitive to the placement of the injection and extraction points, implying that air flow patterns in the tunnel are likely subjected to change through time as changes to the internal geometry of the tunnel were made (Fig. 21).

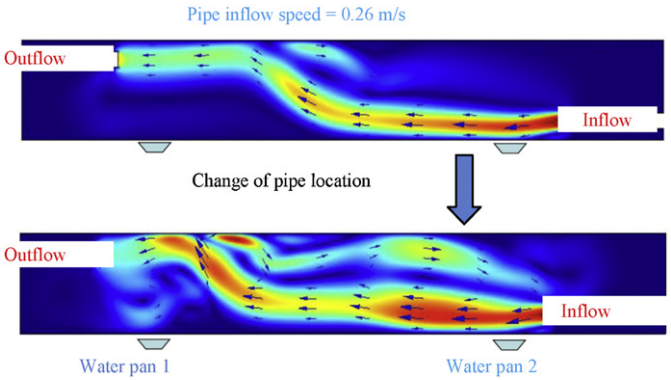


**Fig. 21.** Air flow velocity pattern for two slightly different geometrical configurations of the ventilation experiment tunnel.

It is difficult to draw conclusions from this analysis with regard to the abstracted model approach, as the model shown above does include the water vapour migration and coupling with the Opalinus clay. However, it might suggest that the marginally preferred configuration of reduced radial mixing through a lack of turbulence in the tunnel, when using the abstracted model, might be appropriate in this case.

## 6. Conclusions

One of the key elements of a porous medium drying analysis is the treatment of the surface condition. Furthermore, if genuine predictions are to be made on the HM evolution of the porous media in an argillaceous geological radioactive waste disposal facility, this understanding of the surface condition needs to be coupled with an appropriate treatment of the tunnel itself.

The work presented in this paper has shown that for the Mont Terri VE, multiple approaches to model the tunnel and the surface condition can be successful. Flux-based and pressure-based methods for representing evaporation of liquid water were found to be equivalent within the bounds of data uncertainty for both the drying test and the VE, although the pressure-based method showed significantly higher sensitivity to the assumptions regarding the radial distribution of water vapour in the tunnel.

When modelling the tunnel itself, "abstracted" methods, whereby only the water vapour component of the tunnel system was modelled using *a priori* assumptions on the movement of air, were shown to be remarkably effective in allowing the full tunnel and HM porous media system to be modelled as a single entity. In the case of the VE, this enabled the true experimental boundary conditions of the model to be reflected in the analysis.

## Acknowledgements

The work described in this paper was conducted within the context of the international DECOVALEX Project (DEmonstration of COupled models and their VALidation against EXperiments). The authors are grateful to the Funding Organisations who supported the work. Quintessa Ltd. and University of Edinburgh were supported by the Nuclear Decommissioning Authority (NDA), UK; CEA was supported by Institut de Radioprotection et de Sûreté Nucléaire (IRSN). The Japan Atomic Energy Agency (JAEA) and the Institute of Rock and Soil Mechanics, Chinese Academy of Sciences (CAS) funded DECOVALEX and participated in the work.

The views expressed in the paper are, however, those of the authors and are not necessarily those of the Funding Organisations. The data used in this work were obtained in the framework of the EC project NF-PRO (Contract number FI6W-CT-2003-02389) under the coordination of ENRESA (Empresa Nacional de Residuos Radiactivos).

## References

Bishop AW. The principle of effective stress. Tecnisk Ukeblad 1959;106(39):859–63.
Bossart P, Nussbaum C. Mont Terri project—heater experiment, engineered barrier emplacement and ventilation experiment tests. Wabern: Swiss Geological Survey; 2007.
Bond A, Benbow S, Wilson J, Millard A, Nakama S, English M, McDermott C, Garitte B. Reactive and non-reactive transport modelling in partially water saturated argillaceous porous media around the ventilation experiment, Mont Terri. Journal of Rock Mechanics and Geotechnical Engineering 2013;5(1).
Floría E, Sanz FJ, García-Siñeriz JL. Drying test: evaporation rate from core samples of "Opalinus clay" under controlled environmental conditions. Project Deliverable 6 EC Contract FIKW-CT2001-00126; 2002.
Garitte B, Bond A, Millard A, Zhang C, Mcdermott C, Nakama S, Gens A. Analysis of hydro-mechanical processes in a ventilated tunnel in an argillaceous rock on the basis of different modelling approaches. Journal of Rock Mechanics and Geotechnical Engineering 2013;5(1), 1.
Garitte B, Gens A, Liu Q, Liu X, Millard A, Bond A, McDermott C, Fujita T, Nakama S. Modelling benchmark of a laboratory drying test in Opalinus Clay. In: Zhao J, Labiouse V, Dudt JP, Mathier JF, editors. Rock mechanics in civil and environmental engineering. Lausanne: CRC Press; 2010. p. 767–70.
Maul PR, Benbow SJ, Bond AE, Robinson PC, Watson CE. The Quintessa multiphysics general-purpose code QPAC. Ver. 2.0. Warrington, UK: Quintessa Report QRS 3000B 8; 2010.
Millard A, Bond AE, Nakama S, Zhang C, Barnichon JD, Garitte B. Accounting for anisotropic effects in the prediction of the hydro-mechanical response of a ventilated tunnel in an argillaceous rock. Journal of Rock Mechanics and Geotechnical Engineering 2013;5(2):97–109.
Muñoz JJ, Lloret A, Alonso E. Characterization of hydraulic properties under saturated and non saturated conditions. UPC: Project Deliverable 4, EC Contract FIKW-CT2001-00126; 2003.
Rutqvist J, Noorishad J, Tsang CF. Coupled thermo-hydromechanical analysis of a heater test in unsaturated clay and fractured rock at Kamaishi mine. SKI: SKI Report 99:50; 1999.
Zhang C, Liu X, Liu Q. A THMC formulation for modelling water transport around a ventilated tunnel in an argillaceous rock. Journal of Rock Mechanics and Geotechnical Engineering 2013;5(2):145–55.

**Dr Alexander Bond** has a background in Natural Sciences, Geology (MA; University of Cambridge, UK) and Hydrogeology (MSc, PhD; University of Birmingham, UK), working as an applied scientist in the arenas of nuclear legacy management, underground natural gas storage and carbon dioxide sequestration. His primary research interests relate to complex coupled process analysis, particularly regarding thermo-hydro-mechano-chemical representations of porous media. Of particular importance to him is the often overlooked art of conceptual and process modelling required to underpin and make sense of nearly all sophisticated numerical analyses. In addition to this background in fundamental process modelling, Alex has also been heavily involved in the development and production of a number of radioactive waste disposal safety cases and performance assessments. The pragmatic but robust representation of complex coupled processes in total systems models of the type regularly used to support safety assessments is a major area of work, attempting to tie together the realities of modern engineering and science and the requirements of stakeholders and regulators. He continues to address issues around radioactive and non-radioactive contaminated land management and provides technical support to a range of geological industries. Alexander Bond is presently employed as a Principal Consultant at Quintessa Ltd., UK (www.quintessa.org) where he is responsible for supporting clients in international research projects such as FORGE and DECOVALEX-2015, as well as his international client-based work.